

Spreading processes with layer-dependent population heterogeneity over multilayer networks

Yurun Tian and Osman Yağın

Department of Electrical and Computer Engineering
Carnegie Mellon University, Pittsburgh, PA, 15213 USA
{yurunt, oyagan}@andrew.cmu.edu

Abstract—The study of spreading processes on complex networks has gained significant attention recently. For example, bond percolation models considering population heterogeneity have been used to provide insights into disease spread and misinformation control. However, most of these studies focus on single-layer contact networks. In our work, we examine how the spreading process is impacted by the existence of multiple contact network layers, considering layer-dependent population heterogeneity from a principled, mathematical perspective. Using SIR dynamics, we derive expressions for three key epidemiological measures: the probability of emergence, the epidemic threshold, and the expected epidemic size. Through extensive simulations, we demonstrate that our analytical results match the numerical results near-perfectly in the finite node regime. These findings reveal the interplay among the multi-layer network structures, transmission dynamics, and population heterogeneity in determining the final outcome of the spreading process. Furthermore, we investigate the impact of layer-dependent population heterogeneity and identify important factors for developing effective and economical layer-oriented spreading control strategies. Overall, our work provides insights into developing and analyzing mitigation and control strategies for disease spread and information diffusion across multi-layer complex networks.

Index Terms—Heterogeneous bond percolation, Branching Process, Population Heterogeneity, Multi-layer networks, Network Epidemics

I. INTRODUCTION

The attention towards studies on spreading processes over complex networks has grown in recent years, driven by the impact of pandemics like COVID-19 and SARS, as well as concerns regarding misinformation diffusion [2]. Researchers have extensively examined mathematical models over complex networks to provide insights into the dynamics of spreading pathogens or information [3]–[6]. The susceptible-infectious-recovered (SIR) compartmental model, in particular, has received significant interest due to its ability to capture the propagation of both pathogens and information [7]–[9]. Additionally, its steady-state analysis is closely linked to *bond-percolation* over networks [9], [10].

More recently, there has been interest on studying the SIR spreading process with increasing complexity of the

underlying contact network (e.g., clustered networks [11]–[13] and multi-layer networks [8], [14], [15]) and the *heterogeneity* [9], [16] of the population. For example, Tian et al. [16] investigated a SIR model with population heterogeneity that manifest from different types of masks that the individuals in the population might be wearing. More broadly, population heterogeneity can also arise from factors such as age, gender, socio-economic status, and access to healthcare and other resources [17]–[19] in the population. In the context of information diffusion, population heterogeneity becomes relevant as individuals may exhibit different tendencies in accepting and transmitting information based on their personalities and fact-checking behaviors [2], [20]. Allard et al. [7] also studied the SIR model with population heterogeneity and showed that their steady-state can be analyzed through a *semi-directed* bond percolation model.

This paper is motivated by the fact that most studies on spreading processes with population heterogeneity consider single-layer networks. However, most real-world spreading processes take place over *multi-layer* networks. In viral spreading, different layers might represent viral spreading paths in different environments, e.g., community, school, workplace, etc, each with a different rate of viral transmissibility [21]. Similarly, (mis)information tends to spread over multiple social media platforms, each with different rates and dynamics of propagation. To the best of our knowledge, there have only been a few prior efforts [7], [22] on studying the SIR model while incorporating *both* population heterogeneity *and* the multi-layer nature of the contact network. Bongiorno and Zino [22] proposed a model that incorporates both population heterogeneity and a multi-layer contact network, but they do not provide mathematical analysis for the three epidemic quantities and instead rely on simulation results. The work by Allard et al. [7] considers multi-type networks with arbitrary joint degree distribution. However, their work does not provide a detailed analysis of the impact of multi-layer network structures and the associated multi-layer transmission dynamics on the final spreading results. Our preliminary work [1] studied the *multi-layer mask model*, which takes into account both population heterogeneity and multi-layer contact network. However, it only considers layer-independent population heterogeneity and thus lacks the capability to investigate mitigation strategies that target specific layers, e.g., in some regions, masks are mandated at school but not communities during pandemics [23].

This work was supported in part by the National Science Foundation through grants CCF-1813637 and CCF-2225513, and the Army Research Office through grant # W911NF-22-1-0181.

Part of the work is to be presented in IEEE Global Communications Conference 2023 [1].

Inspired by these, our main contribution is to provide a thorough analysis of the spreading process in a class of multi-layer networks considering layer-dependent population heterogeneity. For illustrative purposes, we suppose population heterogeneity results from different types of masks (with different efficiencies) that individuals are wearing in the viral spreading context; we also reserve one *mask-type* to represent individuals who do not wear any mask. We present the analytical solution of the multi-layer mask model for three key epidemiological quantities: probability of emergence (PE), epidemic threshold, and expected epidemic size (ES). *Epidemics* refer to *large-scale* spreading events such as viral pandemics or information *memes*. The *emergence of epidemics* represents situations where the spreading process leads to a positive fraction of the population being infected in the limit of the number of nodes going to infinity. Our analytical solutions disentangle the impact of multiple factors, including the multi-layer network structure, transmission dynamics, and layer-dependent population heterogeneity distribution, on these three quantities of interest.

Utilizing the analytical results, we first compare the dynamics of multi-layer networks and their monoplex (single-layer) projections. There has been recent interest [15] in understanding whether monoplex projection of a multi-layer network can still capture the essential properties of a spreading process. We find that projecting a multi-layer network into a single-layer network leads to significant differences in the dynamics warranting a separate multi-layer network structure analysis. Second, we explore layer-dependent population heterogeneity by investigating layer-oriented mitigation control policies. A comparison metric quantifying the expected cost of mask allocation is proposed and has been shown useful in characterizing different layer-oriented mitigation policies. We identify the *transmission power* of each layer in the multi-layer contact network, and the participation rate of nodes in the secondary layer as two crucial factors in developing *effective* and *economical* mitigation strategies. We believe these results provide fundamental insights into the spreading process over multi-layer complex networks when taking into account population heterogeneity. Thus, they might help develop mitigation and control strategies for disease spread and information diffusion.

The structure of this paper is as follows. In Sec. II, we formally describe the multi-layer contact network model and the layer-dependent population heterogeneity model. Sec. III contains our theoretical analysis, where we derive expressions for the probability of emergence, the epidemic threshold, and the expected size of the epidemic. Our theoretical results are verified in Sec. IV, where our analytical results show a near-perfect match with the simulation results. Sec. V compares the single-layer and multi-layer networks. Sec. VI explores layer-dependent population heterogeneity by investigating several layer-oriented mitigation control strategies. Finally, we conclude and discuss future avenues of research in Sec. VII.

II. MODEL

A. Contact network model

Next, we introduce the multi-layer contact network model. For simplicity, we present a two-layer network model that can generalize to networks with more than two layers. We consider a two-layer contact network generated as follows. Consider a population of size n with individuals labeled as $\mathcal{N} = \{1, \dots, n\}$. An edge exists between two nodes if there is a chance to transmit the spreading item (e.g., a piece of news, a virus) between them once in contact. The pattern of these potential transmission-causing contacts forms a network. Let \mathbb{C} represent the first contact layer defined on the node set \mathcal{N} . Let \mathbb{S} represent the second contact layer with the assumption that each node in \mathcal{N} is a member of \mathbb{S} with probability $\alpha \in (0, 1]$. Formally, we let

$$\mathbb{P}[i \in \mathcal{N}_S] = \alpha, \quad i = 1, \dots, n \quad (1)$$

where \mathcal{N}_S denotes the set of individuals who also participate the school layer. Edges belonging to network \mathbb{C} (resp., \mathbb{S}) are noted as type- c (resp. type- s) edges.

We generate network \mathbb{C} and \mathbb{S} independently via the *configuration model* in line with prior work on stochastic epidemic models [24], [25]. In other words, the network topology is generated *randomly* from the given degree distribution. The degree distributions for \mathbb{C} and \mathbb{S} are given as $\{p_k^c\}$ and $\{p_k^s\}$, where $k = 0, 1, \dots$. p_k^c (resp. p_k^s) denotes the probability that an arbitrary node on network \mathbb{C} (resp. \mathbb{S}) has degree k , i.e., it is connected to k other nodes via an *undirected* type- c (resp. type- s) edge. We assume the degree distributions are *well-behaved*, i.e., their moments of arbitrary order are *finite* [25] (e.g., Poisson degree distributions, power law degree distributions with exponential cut-off, etc.).

We describe the procedure of generating layer \mathbb{C} given its degree distribution $\{p_k^c\}$ using the configuration model. Generation of layer \mathbb{S} is similar. First, we draw a set of random numbers of size n from the degree distribution $\{p_k^c\}$, denoted as $\{k_c^i\}, i = 1, \dots, n$. Stubs of type- c edges emerging from node i is given as k_c^i . Then we randomly choose pairs of these stubs and place edges on the graph joining them up. This requires the sum $\sum_{i=1}^n k_c^i$ to be even because each edge added to the graph must have two ends. We draw a new set if the set $\{k_c^i\}$ sum to an odd number.

After generating layer \mathbb{C} and layer \mathbb{S} independently, the multi-layer network \mathbb{H} is formed by taking the *disjoint* union of \mathbb{C} and \mathbb{S} , i.e., $\mathbb{H} = \mathbb{C} \amalg \mathbb{S}$. In this setting, an arbitrary node i in \mathcal{N} will have a *colored* degree represented by an integer vector $\mathbf{d}^i = [k_c^i, k_s^i]$, where k_c^i (resp., k_s^i) stands for its number of type- c edges (resp. type- s). The colored degree distribution for node i is thus given by:

$$p_{\mathbf{d}^i} = \left(\alpha p_{k_s^i}^s + (1 - \alpha) \mathbf{1}[k_s^i = 0] \right) \cdot p_{k_c^i}^c, \quad \mathbf{d}^i = (k_c^i, k_s^i). \quad (2)$$

where the term $(1 - \alpha) \mathbf{1}[k_s^i = 0]$ accounts for the case where node i is not a member of layer \mathbb{S} , and its number of type- s edges is automatically zero. Following, we denote random graphs \mathbb{C} and \mathbb{S} as $\mathbb{C}(n, \{p_k^c\})$ and $\mathbb{S}(n; \alpha, \{p_k^s\})$, respectively.

B. Layer-dependent population heterogeneity

In their seminal work [9], Newman studied the SIR (susceptible-infectious-recovered) model over a contact network generated by the configuration model through bond percolation theory. Newman's model captures complex viral transmission mechanisms via the average transmissibility parameter T . Many works have since incorporated various node-level heterogeneity based on Newman's model [1], [16], [18], among which Tian and Yağan [1] studied a SIR model with layer-independent population heterogeneity over multi-layer networks. Specifically, they study a two-layer contact network, where each layer is denoted as layer- \mathbb{C} and layer- \mathbb{S} , respectively. They assume separate baseline transmissibilities T_c and T_s for layer- \mathbb{C} and layer- \mathbb{S} . In other words, T_c and T_s are the probability of transmission (i.e., *transmissibility*) over type- c and type- s edges, respectively. Population heterogeneity is modeled via the inward and outward efficiency of different types of masks that individuals might wear. Assuming that there are M types of masks, the mask distribution is given by $\mathbf{p} = \{p_1, \dots, p_M\}$ where p_i represents the fraction of individuals who wear masks of type- i . Let $\epsilon_{out,i}$ (resp. $\epsilon_{in,i}$) denote the outward (resp. inward) efficiency of mask type- i , where $0 \leq \epsilon_{out,i} \leq 1$ and $0 \leq \epsilon_{in,i} \leq 1$ for all $1 \leq i \leq M$. Two transmissibility matrices \mathbf{T}_c and \mathbf{T}_s , each of size $M \times M$, represent all possible transmissibilities over layer \mathbb{C} and \mathbb{S} , respectively. More specifically,

$$\mathbf{T}_c[i, j] = (1 - \epsilon_{out,i})(1 - \epsilon_{in,j})T_c, \quad 1 \leq i, j \leq M \quad (3)$$

$$\mathbf{T}_s[i, j] = (1 - \epsilon_{out,i})(1 - \epsilon_{in,j})T_s, \quad 1 \leq i, j \leq M \quad (4)$$

where $\mathbf{T}_c[i, j]$ (resp. $\mathbf{T}_s[i, j]$) gives the probability that, an infected node wearing a type- i mask transmits the virus/information to a susceptible node wearing a type- j mask given that they are connected by a type- c (resp. type- s) link.

Assumptions are made regarding population heterogeneity and the corresponding transmission dynamics in Ref. [1]. Mask distribution is assumed to be independent of the network structure and the spreading process. Each node keeps a consistent mask choice across layers. However, in real life, population heterogeneity can be correlated with the network structure. For example, there were times and regions where surgical masks were mandated in schools but not in communities during the COVID-19 pandemic [23]. Similarly, in information spreading, some people are more willing to speak out (or be silent) online than in real life, or vice versa [26]. Modeling layer-dependent population heterogeneity will thus provide a better understanding of the role of the multi-layer network structure in the spreading processes, and assist in developing layer-specific control strategies in mitigating a spreading process.

In this work, we incorporate layer-dependent population heterogeneity by associating node type with the node's layer-dependent mask-wearing behavior. In other words, nodes can exhibit different mask-wearing behaviors in different layers of contact networks. In particular, given $M \geq 1$ different types of masks, an arbitrary node v in the population \mathcal{N} is type- ij if it wears a type- i mask in layer- \mathbb{C} and a type- j mask in layer- \mathbb{S} . This will lead to M^2 node types in total, with the node type

distribution given as $\mathbf{m} = \{m_{ij}\}, 1 \leq i, j \leq M$. Individual node type is independently drawn from this distribution. We assume the node type is pre-assigned before the spreading process starts. We also assume that node type is independent of the multi-layer network structure and does not depend on whether the node participates in layer- \mathbb{S} . We shall see that $p_i = \sum_{j=1}^M m_{ij}$.

For integers $1 \leq i, j, r, t \leq M$, the transmissibility from a type- ij infected node to a type- rt susceptible node is thus given by: $(1 - \epsilon_{out,i})(1 - \epsilon_{in,r})T_c$ if the transmission occurs via a type- c edge, and $(1 - \epsilon_{out,j})(1 - \epsilon_{in,t})T_s$ if the transmission occurs via a type- s edge.

Even though there are M^2 node types, $M \times M$ (rather than $M^2 \times M^2$) possible transmissibilities exist on each layer. This is because the transmissibility for an infectious-susceptible node pair only depends on the corresponding mask types and the baseline transmissibility given the edge type that connects them. Therefore, we continue using the same \mathbf{T}_c and \mathbf{T}_s in (3) and (4) to represent all possible transmissibilities for each layer, but with extended semantics in usage. Specifically, for a type- ij infected node, it transmits the spreading item to a type- rt susceptible node with probability $\mathbf{T}_c[i, r]$ if the transmission occurs over a type- c edge, as with probability $\mathbf{T}_s[j, t]$ if the transmission occurs over a type- s edge, where

$$\mathbf{T}_c[i, r] = (1 - \epsilon_{out,i})(1 - \epsilon_{in,r})T_c, \quad 1 \leq i, r \leq M \quad (5)$$

$$\mathbf{T}_s[j, t] = (1 - \epsilon_{out,j})(1 - \epsilon_{in,t})T_s, \quad 1 \leq j, t \leq M \quad (6)$$

III. ANALYTICAL RESULTS

This section presents the derivation of the probability of emergence (PE), the epidemic threshold, and the expected epidemic size (ES). *Emergence* is defined as the event where the spreading process leads to a positive fraction of the infected population in the limit of the number of nodes n going to infinity. *Epidemics* refer to *large-scale* spreading events such as viral pandemics or information *memes*. Formally, with $S(n)$ denoting the *final* fraction of infected nodes in the population size of n , the probability of emergence with a random initiator is given by $\text{PE} = \lim_{n \rightarrow \infty} \mathbb{P}[S > 0]$. Further, we are also interested in the epidemic threshold that separates the parameter space where $\lim_{n \rightarrow \infty} \mathbb{P}[S > 0] = 0$ from those that yield $\lim_{n \rightarrow \infty} \mathbb{P}[S > 0] > 0$. Finally, we compute the expected epidemic size when they take place, i.e., $\lim_{n \rightarrow \infty} \mathbb{E}[S | S > 0]$.

A. Probability of Emergence and Epidemic Threshold

Consider random graphs $\mathbb{C}(n, \{p_k^c\})$ and $\mathbb{S}(n; \alpha, \{p_k^s\})$ as introduced in Section II-A. In order to study the viral transmission in the multi-layer network $\mathbb{H} = \mathbb{C} \amalg \mathbb{S}$, we consider a branching process that starts by giving the pathogen to an arbitrary node and the recursively identify the set of nodes that are reached and *infected* by exploring its neighbors. As mentioned in Section II-B, a type- ij infected node transmits the pathogen to a type- rt susceptible neighbor with probability $\mathbf{T}_c[i, r] = T_c(1 - \epsilon_{i,out})(1 - \epsilon_{r,in})$ if the link connecting them is type- c (or, with probability $\mathbf{T}_s[j, t] = T_s(1 - \epsilon_{j,out})(1 - \epsilon_{t,in}$

if the link between them is type- s), independently from all other neighbors.

The *survival probability* of the aforementioned branching process is derived through a *mean-field* approach utilizing the method of generating functions [9], [25]. For integers $1 \leq i, j, r, t \leq M$, let $h_{c,ij}(x)$ (resp. $h_{s,ij}(x)$) denote the generating function for “the *finite* number of nodes reached and infected by following a *randomly* selected type- c (resp. type- s) edge coming from a type- ij infected node.” Put differently, we have $h_{c,ij}(x) = \sum_{m=0}^{\infty} v_m x^m$ where v_m denotes the “probability that an arbitrary type- c edge coming from a type- ij infected node leads to a component of size m .” Similarly, let $H_{ij}(x)$ denote the generating function for “the finite number of nodes reached and infected by following a randomly selected type- ij node.”

Now we derive $h_{c,ij}(x)$ and $h_{s,ij}(x)$. For integers $1 \leq i, j, r, t \leq M$, we find that the following $2M^2$ self-consistency equations hold:

$$h_{c,ij}(x) = \sum_{r=1}^M \sum_{t=1}^M m_{rt} \left(1 - \mathbf{T}_c[i, r] + \mathbf{T}_c[i, r] x \sum_{\mathbf{d}} \frac{p_{\mathbf{d}} k_c}{\langle k_c \rangle} h_{c,rt}(x)^{k_c-1} h_{s,rt}(x)^{k_s} \right) \quad (7)$$

$$h_{s,ij}(x) = \sum_{r=1}^M \sum_{t=1}^M m_{rt} \left(1 - \mathbf{T}_s[j, t] + \mathbf{T}_s[j, t] x \sum_{\mathbf{d}} \frac{p_{\mathbf{d}} k_s}{\langle k_s \rangle} h_{c,rt}(x)^{k_c} h_{s,rt}(x)^{k_s-1} \right) \quad (8)$$

We now explain each term in (7). Consider an infected type- ij node, say node v , and consider a type- c edge incident on it. We condition on the *type* of the node on the other end of this edge, say node u . Since the node type assignment is completed before the spreading process and is drawn independently for all the nodes, the direct neighbor node u is of type- rt with probability m_{rt} . Conditioning on node u being type- rt , it will become infected through the type- c edge from v , with probability $\mathbf{T}_c[i, r]$. If the transmission fails with probability $1 - \mathbf{T}_c[i, r]$, then node v will have zero offspring through this edge to u , which explains the first part of (7). If the transmission is successful with probability $\mathbf{T}_c[i, r]$, the number of nodes reached and infected by node v increases by one (i.e., node u). This is captured by the multiplicative term x in the second half of (7). Additionally, the total size of this branch will also include all subsequent nodes that are reached and infected by u , which leads to the following term:

$$\sum_{\mathbf{d}} \frac{p_{\mathbf{d}} k_c}{\langle k_c \rangle} h_{c,rt}(x)^{k_c-1} h_{s,rt}(x)^{k_s}.$$

This term is explained as follows. First, we condition on the *colored degree* of node u , i.e., number of edges in both network layers. The term $p_{\mathbf{d}} k_c / \langle k_c \rangle$ gives the probability that the *colored degree* of u is \mathbf{d} [9]. It is the normalized probability that a type- c edge is attached to a node at the other end with colored degree $\mathbf{d} = (k_c, k_s)$. Therefore, following the type- c edge from v that reaches u , u can infect other nodes with the remaining $k_c - 1$ edges of type- c and k_s edges of type- s . Recall that the number of nodes reached and infected by a

type- rt node by following a type- c (resp. type- s) edge attached is generated by $h_{c,rt}$ (resp. $h_{s,rt}$). Collecting all the sub-branches, we obtain the term $h_{c,rt}(x)^{k_c-1} h_{s,rt}(x)^{k_s}$ utilizing the *powers property* of generating functions [25]. The validity of (8) can be seen in a very similar way and is omitted here for brevity.

Utilizing (7) and (8), we now derive the generating function $H_{ij}(x)$ for the entire size of the branching process. For $1 \leq i, j \leq M$, we have

$$H_{ij}(x) = x \sum_{\mathbf{d}} p_{\mathbf{d}} h_{c,ij}(x)^{k_c} h_{s,ij}(x)^{k_s} \quad (9)$$

Here, the factor x corresponds to the initial node selected arbitrarily and infected. The selected node has colored degree $\mathbf{d} = (k_c, k_s)$ with probability $p_{\mathbf{d}}$. The number of nodes it reaches and infects by each of its k_c (resp. k_s) links of type- c (resp. type- s) is generated through $h_{c,ij}(x)$ (resp. $h_{s,ij}(x)$). Summing over all the possible colored degrees, we obtain (9).

With (7)-(9) in hand, the generating function $H_{ij}(x)$ can be computed in the following manner. Given any x , we can solve for the recursive relations (7)-(8) to obtain $h_{c,ij}(x)$ and $h_{s,ij}(x)$ for integers $1 \leq i, j \leq M$, which in turn will yield $H_{ij}(x)$ for integers $1 \leq i, j \leq M$ in light of (9).

We are interested in cases where the number of nodes reached and infected by the initial node is *infinite*, representing cases where a randomly chosen infected node triggers an *epidemic*. The *conservation of probability* property of generating functions indicates that there exists a trivial fixed point $h_{c,ij}(1) = h_{s,ij}(1) = 1$ (yielding $H_{ij}(1) = 1$) when the number of nodes reached and infected is always *finite*. In other words, the underlying branching process is in the *sub-critical* regime, and *all* infected components have finite size. However, the fixed point $h_{c,ij}(1) = h_{s,ij}(1) = 1$ may not be a stable solution to the recursion (7) to (9).

We can check the stability of this fixed point by the linearization of recursion (7) to (9) around $h_{c,ij}(1) = h_{s,ij}(1) = 1$, $1 \leq i, j, r, t \leq M$. This yields the Jacobian matrix \mathbf{J} with the form $\mathbf{J} = \begin{bmatrix} \mathbf{J}_{cc} & \mathbf{J}_{cs} \\ \mathbf{J}_{sc} & \mathbf{J}_{ss} \end{bmatrix}_{2M^2 \times 2M^2}$ in which

$$\begin{aligned} \mathbf{J}_{cc}(a, b) &= \frac{\partial h_{c,ij}(1)}{\partial h_{c,rt}(1)}; & \mathbf{J}_{cs}(a, b) &= \frac{\partial h_{c,ij}(1)}{\partial h_{s,rt}(1)} \\ \mathbf{J}_{ss}(a, b) &= \frac{\partial h_{s,ij}(1)}{\partial h_{s,rt}(1)}; & \mathbf{J}_{sc}(a, b) &= \frac{\partial h_{s,ij}(1)}{\partial h_{c,rt}(1)} \end{aligned} \quad (10)$$

where $a = \text{M2D}(i, j), b = \text{M2D}(r, t), 1 \leq i, j, r, t \leq M$. M2D is an M -base to 10-base converter to map the tuple $ij, 1 \leq i, j \leq M$ to an integer ranging from 1 to M^2 for the ease of matrix indexing. The four sub-matrices in (10), i.e., \mathbf{J}_{cc} to \mathbf{J}_{ss} are each of the shape $M^2 \times M^2$. For example, when we consider taking the derivative of $h_{c,ij}(x)$ in (7) with respect to one of its inputs $h_{c,rt}(x)$ when $x = 1$ (denoted by $\frac{\partial h_{c,ij}(1)}{\partial h_{c,rt}(1)}$), the result corresponds to an element in the matrix \mathbf{J}_{cc} with coordinates (a, b) , where $a = \text{M2D}(i, j)$ and $b = \text{M2D}(r, t)$ are integers within $1 \leq a, b \leq M^2$. Without loss of generality, we place the order of the four sub-matrices \mathbf{J}_{cc} to \mathbf{J}_{ss} as above. Swapping the locations of the sub-matrices will not change the spectral radius of \mathbf{J} because two of the sub-matrices can always commute and thus share

the same polynomial characteristics based on [27, Thm 3]. We will use this property again to show PE and ES share the same transition points later in Appendix Sec. A.

If all eigenvalues of \mathbf{J} are less than one in absolute value, i.e., if the spectral radius $\rho(\mathbf{J})$ of \mathbf{J} satisfies $\rho(\mathbf{J}) \leq 1$, then the solution $h_{c,ij}(1) = h_{s,rt}(1) = 1$ is stable and $H_{ij}(1) = 1$ becomes the physical solution for all $1 \leq i, j \leq M$. In this case, the fraction of infected nodes will tend to zero as the number of nodes n goes to infinity. In contrast, if $\rho(\mathbf{J}) > 1$, the trivial fixed point is not stable, which indicates that the branching process is in the *supercritical* regime; i.e., there is a positive probability that the branching process will lead to an *infinite* component. In this case, the fraction of nodes that are infected will be strictly greater than zero as the number of nodes n goes to infinity.

When $\rho(\mathbf{J}) > 1$, a nontrivial fixed point exists and becomes the attractor of the recursions (7) to (9), leading to a solution with $h_{c,ij}(1), h_{s,ij}(1) < 1$ which in turn yields $H_{ij}(1) < 1$. In that case, $1 - H_{ij}(1)$ gives the probability that the spreading process initiated by a seed node of type- ij yields an *epidemic*. Recall that S denotes the *final* fraction of infected nodes. The probability of epidemic emergence PE (with a random initiator) is thus given by $\text{PE} = \lim_{n \rightarrow \infty} \mathbb{P}[S > 0] = \sum_{i,j=1}^M m_{ij}(1 - H_{ij}(1))$. Finally, we conclude that the epidemic threshold, i.e., the boundary that separates the parameter regions where $\lim_{n \rightarrow \infty} \mathbb{P}[S > 0] = 0$ from those that yield $\lim_{n \rightarrow \infty} \mathbb{P}[S > 0] > 0$ is given by $\rho(\mathbf{J}) = 1$.

To further look into the implications of (10), utilizing (7) to (8), we have

$$\begin{aligned} \mathbf{J}_{cc} &= [\lambda_{cc} \cdot \mathbf{T}'_c \cdot \mathbf{m}]; & \mathbf{J}_{cs} &= [\lambda_{cs} \cdot \mathbf{T}'_c \cdot \mathbf{m}] \\ \mathbf{J}_{sc} &= [\lambda_{sc} \cdot \mathbf{T}'_s \cdot \mathbf{m}]; & \mathbf{J}_{ss} &= [\lambda_{ss} \cdot \mathbf{T}'_s \cdot \mathbf{m}] \end{aligned} \quad (11)$$

$$\begin{aligned} \lambda_{cc} &= \frac{\langle k_c^2 \rangle - \langle k_c \rangle}{\langle k_c \rangle}, & \lambda_{cs} &= \frac{\langle k_c k_s \rangle}{\langle k_c \rangle} \\ \lambda_{ss} &= \frac{\langle k_s^2 \rangle - \langle k_s \rangle}{\langle k_s \rangle}, & \lambda_{sc} &= \frac{\langle k_c k_s \rangle}{\langle k_s \rangle} \end{aligned}$$

where $\mathbf{T}'_c[a, b] = \mathbf{T}_c[i, r]$, $\mathbf{T}'_s[a, b] = \mathbf{T}_c[j, t]$, $\mathbf{m} = \text{diag}(\mathbf{m})$, where $\mathbf{m}[a, a] = \mathbf{m}[i, j]$, $a = \text{M2D}(i, j)$, $b = \text{M2D}(r, t)$, $1 \leq i, j, r, t \leq M$. Here \mathbf{m} is a diagonal matrix of the node type distribution $\mathbf{m} = \{m_{ij}\}$. In matrix \mathbf{T}'_c (resp. \mathbf{T}'_s), each element in \mathbf{T}_c (resp. \mathbf{T}_s) will be at least duplicated for M^2 times. \mathbf{T}'_c and \mathbf{T}'_s are functions of the mask efficiencies and baseline transmissibilities, encoding all possible transmission scenarios when taking into account layer-dependent population heterogeneity over layer- \mathbb{C} and \mathbb{S} , respectively. Note \mathbf{T}'_c and \mathbf{T}'_s are not symmetric unless \mathbf{T}_c and \mathbf{T}_s are symmetric, which only holds on when $\mathbf{1} - \epsilon_{\text{out}}$ and $\mathbf{1} - \epsilon_{\text{in}}$ are colinear.

Observe that the four sub-matrices of \mathbf{J} in (11) follow the same pattern, i.e., they are composed of three parts from left to right: i) a parameter that attributes the multi-layer network structure; ii) a heterogeneous edge-type and node-type dependent transmissibility term; and iii) a node type distribution term. This result disentangles the impact of multiple factors on the final state of the spreading process: the degree distribution of different layers of the contact network

as a whole, viral transmission dynamics, and layer-dependent population heterogeneity.

In the special case where population heterogeneity is layer-independent, \mathbf{T}_c and \mathbf{T}_s are rank-1 and can be decomposed into $T_c \cdot \epsilon_{\text{out}} \cdot \epsilon_{\text{in}}^\top$ and $T_s \cdot \epsilon_{\text{out}} \cdot \epsilon_{\text{in}}^\top$, respectively. In other words, the node type here is not correlated with the network structure, and $\epsilon_{\text{out}} \cdot \epsilon_{\text{in}}^\top$ is a property of each type of masks. The Jacobian matrix for the layer-independent population heterogeneity can be further simplified as follows:

$$\left[\begin{array}{cc} T_c & \\ & T_s \end{array} \right] \cdot \left[\begin{array}{cc} \lambda_{cc} & \lambda_{cs} \\ \lambda_{sc} & \lambda_{ss} \end{array} \right] \otimes \left((\mathbf{1} - \epsilon_{\text{out}}) \cdot (\mathbf{1} - \epsilon_{\text{in}}^\top) \cdot \mathbf{p} \right) \quad (12)$$

where $\mathbf{p} = \text{diag}(\mathbf{p})$ (recall \mathbf{p} is mask type distribution), and \otimes is the Kronecker product sign. The spectral radius $\rho(\mathbf{J})$ is thus

$$\rho \left(\left[\begin{array}{cc} T_c & \\ & T_s \end{array} \right] \cdot \left[\begin{array}{cc} \lambda_{cc} & \lambda_{cs} \\ \lambda_{sc} & \lambda_{ss} \end{array} \right] \right) \cdot \rho \left((\mathbf{1} - \epsilon_{\text{out}}) \cdot (\mathbf{1} - \epsilon_{\text{in}}^\top) \cdot \mathbf{p} \right) \quad (13)$$

The expression (13) further disentangles the network-related and mask-related factors and shows the trade-off between them upon the critical behavior of the spreading process. From (13), it is straightforward to derive the spectral radius for the *single* layer network that has degree distribution $\{p_k\}$ with mean degree $\langle k \rangle$ and baseline transmissibility T with population heterogeneity by the same set of masks. Namely, (14). This expression was obtained in [18] for single-layer contact networks.

$$\rho(\mathbf{J}_{\text{single-layer}}) = \frac{\langle k^2 \rangle - \langle k \rangle}{\langle k \rangle} \cdot T \cdot \rho \left((\mathbf{1} - \epsilon_{\text{out}}) \cdot (\mathbf{1} - \epsilon_{\text{in}}^\top) \cdot \mathbf{p} \right) \quad (14)$$

B. Expected epidemic size

In this section, we compute the expected size of epidemics when they take place, i.e., $\lim_{n \rightarrow \infty} \mathbb{E}[S \mid S > 0]$. We will also compute the fraction of infected nodes in each type. Our approach is similar to that used in [1], [4], [5], [18], [28]. Since the multi-layer network \mathbb{H} is locally tree-like as the network size approaches infinity [29], we can consider it as a tree-structure, where there is a single node of type- ij at the top level (referred to as the *root*). We label the levels of the tree from $\ell = 0$ at the bottom to $\ell = \infty$ at the top. Without loss of generality, we assume that the spreading event starts at the bottom of the tree and proceeds toward the top. In other words, we assume that a node at level $\ell + 1$ can only be infected by one of its neighbors in level ℓ . Let $q_{c,\ell}^{ij}$ (respectively, $q_{s,\ell}^{ij}$) denote the probability of a type- ij node at level ℓ who is connected to its parent at level $\ell + 1$ through a type- c (respectively, type- s) edge is *not* infected. Our goal is to compute q_{∞}^{ij} which represents the probability that the *root* node, which is of type- ij , is *not* infected. Given that the root node is arbitrary, q_{∞}^{ij} also gives the expected fraction of type- ij nodes that will not be infected during the spreading process. Put differently, we have $\lim_{n \rightarrow \infty} \mathbb{E}[S_{ij} \mid S > 0] = 1 - q_{\infty}^{ij}$ with S_{ij} denoting the fraction of nodes of type- ij that are infected in the spreading process; we also have $\mathbb{E}[S] = \sum_{i,j=1}^M m_{ij} \mathbb{E}[S_{ij}]$.

Now we derive $q_{c,\ell}^{ij}$ and $q_{s,\ell}^{ij}$ in a recursive manner. For each $i, j = 1, \dots, M$, we find that

$$q_{c,\ell+1}^{ij} = \sum_{\mathbf{d}=(k_c, k_s)} \frac{p_{\mathbf{d}}^{k_c}}{\langle k_c \rangle} f_{ij}(\mathbf{q}_{c,\ell}, \mathbf{q}_{s,\ell}, k_c - 1, k_s) \quad (15)$$

$$q_{s,\ell+1}^{ij} = \sum_{\mathbf{d}=(k_c, k_s)} \frac{p_{\mathbf{d}}^{k_s}}{\langle k_s \rangle} f_{ij}(\mathbf{q}_{c,\ell}, \mathbf{q}_{s,\ell}, k_c, k_s - 1) \quad (16)$$

where $\mathbf{q}_{c,\ell} = [q_{c,\ell}^{11}, q_{c,\ell}^{12}, \dots, q_{c,\ell}^{MM}]$, and

$$f_{ij}(\mathbf{q}_{c,\ell}, \mathbf{q}_{s,\ell}, k_c, k_s) = \left(\sum_{r=1}^M \sum_{t=1}^M m_{rt} (1 - \mathbf{T}_c[r, i] + q_{c,\ell}^{rt} \mathbf{T}_c[r, i]) \right)^{k_c} \cdot \left(\sum_{r=1}^M \sum_{t=1}^M m_{rt} (1 - \mathbf{T}_s[t, j] + q_{s,\ell}^{rt} \mathbf{T}_s[t, j]) \right)^{k_s} \quad (17)$$

In order to see why (15) holds, let u be a type- ij node at level $\ell + 1$ who is connected to its unique parent at level $\ell + 2$ with an edge of type- c . As already mentioned, $q_{c,\ell+1}^{ij}$ gives the probability that u is *not* infected. As before, we first condition on the colored degree of u being $\mathbf{d} = (k_c, k_s)$ which has probability $\frac{p_{\mathbf{d}}^{k_c}}{\langle k_c \rangle}$. Under the assumption that nodes can only be infected by neighbors in the layers below, node u can be infected through either one of $k_c - 1$ edges of type- c and k_s edges of type- s in layer ℓ (given that one of its type- c edges is used to connect it to the parent node in layer $\ell + 2$). We establish (15) by noting that $f_{ij}(\mathbf{q}_{c,\ell}, \mathbf{q}_{s,\ell}, k_c, k_s)$ represents the probability that a type- ij node with k_c edges of type- c and k_s edges of type- s with nodes in layer ℓ is *not* infected. The expression (16) can be seen to hold similarly.

We now explain why (17) holds. For a node with k_c edges of type- c and k_s edges of type- s in layer ℓ to be not infected, it should not receive the pathogen from any of these neighbors. Given the independence of infection events, we see that $f_{ij}(\mathbf{q}_{c,\ell}, \mathbf{q}_{s,\ell}, k_c, k_s)$ should be of the form $f_{ij}(\mathbf{q}_{c,\ell})^{k_c} f_{ij}(\mathbf{q}_{s,\ell})^{k_s}$ with $f_{ij}(\mathbf{q}_{c,\ell})$ (respectively, $f_{ij}(\mathbf{q}_{s,\ell})$) defined as the probability that a type- ij node with only one edge of type- c (respectively, type- s) with nodes in layer ℓ is *not* infected. In order to compute $f_{ij}(\mathbf{q}_{c,\ell})$, we condition on the type of the node that is connected in layer ℓ , which is type- rt with probability m_{rt} . Then, we note that a type- ij node in layer $\ell + 1$ will be infected by a type- rt neighbor in layer ℓ that it is connected via a type- c link if both of the following events hold: the node in layer ℓ is infected, which happens with probability $(1 - q_{c,\ell}^{rt})$, and the pathogen is transmitted from the node in layer ℓ to its parent in layer $\ell + 1$, which happens with probability $\mathbf{T}_c[r, i]$. Collecting, we see that the probability of a type- ij node in layer $\ell + 1$ to be *not* infected by a type- rt neighbor in layer ℓ that it is connected via a type- c is given by

$$1 - (1 - q_{c,\ell}^{rt}) \mathbf{T}_c[r, i] = 1 - \mathbf{T}_c[r, i] + q_{c,\ell}^{rt} \mathbf{T}_c[r, i]$$

Proceeding similarly for $f_{ij}(\mathbf{q}_{s,\ell})$, we establish (17).

We are now able to compute $q_{c,\infty}^{ij}$ for each $i, j = 1, \dots, M$. First, solving (15)-(16) in the limit of $\ell \rightarrow \infty$ we compute $\mathbf{q}_{c,\infty}$ and $\mathbf{q}_{s,\infty}$. Using these, we then get

$$q_{c,\infty}^{ij} = \sum_{\mathbf{d}=(k_c, k_s)} p_{\mathbf{d}} f_{ij}(\mathbf{q}_{c,\infty}, \mathbf{q}_{s,\infty}, k_c, k_s) \quad (18)$$

by conditioning on the colored degree of the root node. Finally, we have $\lim_{n \rightarrow \infty} \mathbb{E}[S_{ij} | S > 0] = 1 - q_{c,\infty}^{ij}$ and the expected epidemic size is given by $\text{ES} = \lim_{n \rightarrow \infty} \mathbb{E}[S | S > 0] = \sum_{i,j=1}^M m_{ij} (1 - q_{c,\infty}^{ij})$.

Note the convergence to the fixed point $\mathbf{q}_{c,\infty}$ and $\mathbf{q}_{s,\infty}$ is guaranteed. Moreover, ES and PE share the same phase transition point defined by $\rho(\mathbf{J}) = 1$. More discussion on the convergence guarantee and phase transition can be found in Appendix Section A.

IV. NUMERICAL RESULTS

In this section, we present simulation results in the finite node regime with an eye toward validating our analytical results. Note that the analytical results are exact in the limit of the number of nodes n going to infinity. Throughout, we fix the number of nodes as $n = 10^6$. We run 10,000 independent experiments for each parameter setting and report the average of these independent trials. The network \mathbb{C} and \mathbb{S} are generated based on configuration model using degree distributions with finite moments. We validate our results using two types of degree distributions: Poisson and power law with exponential cutoff. Poisson distribution is chosen for its simplicity and the fact that it is one of the most widely-used and analyzed degree distributions in spreading processes. We choose power law with exponential cutoff distribution, too, because they are applied to a wide range of real-world networks [5], [30], and they are *well-behaved*, i.e., have finite moments.

The fraction of nodes participating in network layer \mathbb{S} is denoted by α . The baseline transmissibilities are denoted by T_c and T_s for networks \mathbb{C} and \mathbb{S} , respectively.

A. Opposite trends between PE and ES

In this experiment, we report an interesting trend that a higher probability of emergence may *not* correspond to a larger expected epidemic size given when the epidemic happens. We assume there are three types of masks: inward-good, outward-good, and no-mask. When the inward efficiency of a mask is better than its outward efficiency, we call them inward-good masks. Similarly, we call masks with higher outward efficiency as outward-good masks. In the viral spread context, inward-good masks are more effective for *self-protection* when the subject is immersed in the environment of virus particles than blocking the virus emitted from the infected person's respiratory system [31]. Similarly, outward-good masks are better at *source control* than the protection of the wearer [32]. We use vectors ϵ_{in} and ϵ_{out} to represent the inward and outward efficiencies for all types of masks. For simplicity, we only consider layer-independent population heterogeneity.

We assume there are three types of individuals in the population: inward-good mask wearers, outward-good

mask wearers, and people who don't wear masks, represented as type-1, type-2, and type-3 nodes, respectively. We have the proportion vector of three types as $\mathbf{m} = [m_{\text{outward-good}}, m_{\text{inward-good}}, m_{\text{no-mask}}]$. We fix the proportion of no-mask-wearers at 0.1, and vary the proportion of outward-good-mask-wearers $m_{\text{outward-good}}$ from 0.1 to 0.9. Based on (13), to compare inward-good and outward-good masks fairly, the parameter choice for the inward-good mask and outward-good mask should follow that $(1 - \epsilon_{\text{out},o})(1 - \epsilon_{\text{in},o}) = (1 - \epsilon_{\text{out},i})(1 - \epsilon_{\text{in},i})$, where $\epsilon_{\text{out},o}$ and $\epsilon_{\text{in},o}$ ($\epsilon_{\text{out},i}$ and $\epsilon_{\text{in},i}$ resp.) represent the outward and inward efficiencies for the outward-good mask (inward-good mask resp.). The efficiency parameters of the masks are selected as $\epsilon_{\text{out}} = [0.7, 0.4, 0]$, and $\epsilon_{\text{in}} = [0.4, 0.7, 0]$.

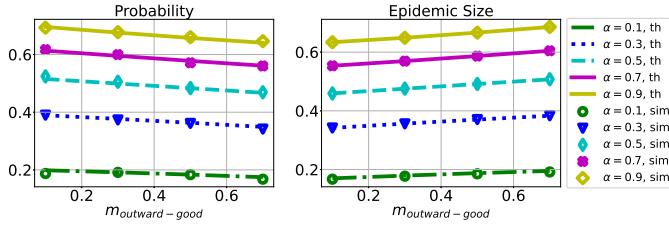


Fig. 1. Probability of emergence (left) and expected epidemic size given emergence (right) show opposite trends as $m_{\text{outward-good}}$ increases. $\epsilon_{\text{out}} = [0.7, 0.4, 0]$, and $\epsilon_{\text{in}} = [0.4, 0.7, 0]$. $m_{\text{no-mask}} = 0.1$. $T_c = 0.6$, $T_s = 0.5$. $\{p_k^c\} \sim \text{Poisson}(6)$, $\{p_k^s\} \sim \text{Poisson}(8)$. Node set size $n = 1,000,000$, and each data point of the simulation result is averaged over 10,000 trials. Analytical results (marked th) show a near-perfect match with the simulation results (marked sim).

Fig. 1 shows that as $m_{\text{outward-good}}$ increases, PE decreases, and ES increases, with different α values. This implies that a source-control-oriented strategy is crucial to prevent the epidemic from emerging over a multi-layer network at the early stages of the virus spreading, i.e., when the infection fraction has not reached a significant percentage. However, if an epidemic has already occurred and a significant fraction of the population has already been infected, it becomes most effective to implement a self-protection-oriented strategy to reduce the final fraction of the infected nodes. This also demonstrates that it is necessary to consider two different phases when considering mitigation strategies for spreading processes. This trend is first reported in Ref. [16] over single-layer networks. Here we validate it over multi-layer networks under different second-layer participation rates.

B. Impact of the node-type distribution

In this experiment, we show how the node-type distribution affects the spreading process, e.g., in terms of probability and expected size of epidemics. We assume there are two types of masks: surgical mask (type-1) and cloth mask (type-2). The outward and inward efficiencies are denoted by $\epsilon_{\text{out}} = [\epsilon_{\text{out},1}, \epsilon_{\text{out},2}]$, and $\epsilon_{\text{in}} = [\epsilon_{\text{in},1}, \epsilon_{\text{in},2}]$. The entire population is thus split into four non-overlapping categories: type-1 on \mathbb{C} and type-1 on \mathbb{S} , type-2 on \mathbb{C} and type-1 on \mathbb{C} and type-2 on \mathbb{S} , and type-2 on \mathbb{C} and type-2 on \mathbb{S} . We let $\mathbf{m} = [m_{11}, m_{21}, m_{12}, m_{22}]$ denote the proportion of the 4 types of nodes. Here we fix $m_{11} = 0.1$, and vary m_{21} and m_{12} , and we set $m_{22} = 0.9 - m_{21} - m_{12}$.

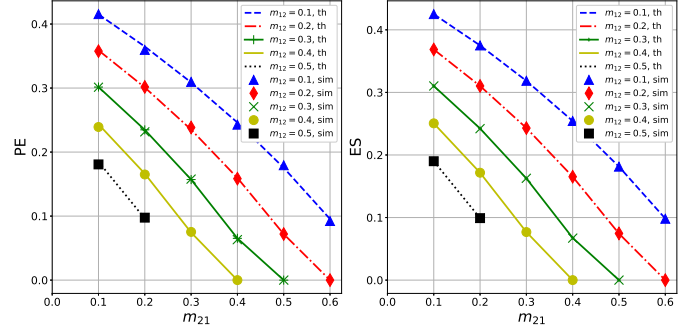


Fig. 2. Probability of emergence (left) and epidemic size given emergence (right) varying m_{21} for different m_{12} values. We set $m_{11} = 0.1$ and $m_{22} = 0.9 - m_{21} - m_{12}$. $\{p_k^c\} \sim \text{Poisson}(6)$, $\{p_k^s\} \sim \text{Poisson}(8)$ and $\alpha = 0.6$. $T_c = 0.6$, $T_s = 0.5$, $\epsilon_{\text{out}} = [0.8, 0.5]$, and $\epsilon_{\text{in}} = [0.7, 0.5]$. Node set size $n = 1,000,000$, and each data point of the simulation result is averaged over 10,000 trials. Analytical results (marked th) show a near-perfect match with the simulation results (marked sim).

In Fig. 2, we investigate how the probability of emergence (PE) and expected epidemic size given emergence (ES) change as we vary m_{21} and m_{12} when the degree distributions are Poisson. We see that the simulation results match the analytical results' usefulness in the finite node regime. Moreover, the results are also helpful in understanding the impact of node-type distributions. It is seen that with fixed m_{11} and m_{12} , as m_{21} increases (m_{22} decreases), PE and ES decrease. Namely, while the fraction of nodes wearing cloth masks on layer- \mathbb{C} and surgical masks on layer- \mathbb{S} increases, PE and ES decrease. This shows that masks with better efficiencies on layer- \mathbb{S} help in reducing the risk and size (if it already exists) of an epidemic. On the other hand, with fixed m_{11} and m_{21} , increasing m_{12} (decreasing m_{22}) decreases PE and ES. Similarly, this indicates that better masks on layer- \mathbb{C} are also helpful. In Sec. VI, we further investigate the interplay between the node-type distribution and multi-layer network structure.

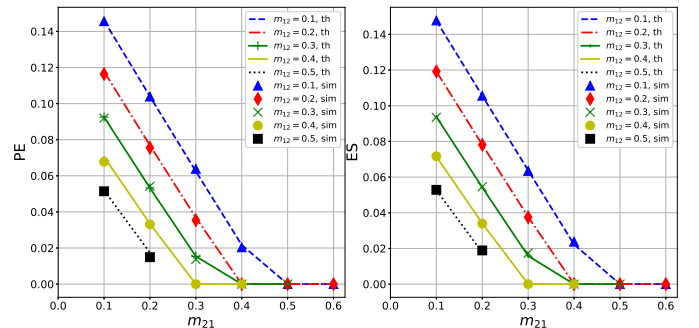


Fig. 3. Probability of emergence (left) and epidemic size given emergence (right) varying m_{21} for different m_{12} values. We set $m_{11} = 0.1$ and $m_{22} = 0.9 - m_{21} - m_{12}$. $\{p_k^c\}$ and $\{p_k^s\}$ follow power law with exponential cutoff where the power exponent equals 2.5, and the cutoff equals 10. The mean degree is 1.028. We set $\alpha = 0.6$. $T_c = 0.4$, $T_s = 0.7$, $\epsilon_{\text{out}} = [0.5, 0]$, and $\epsilon_{\text{in}} = [0.4, 0]$. Node set size $n = 1,000,000$, and each data point of the simulation result is averaged over 10,000 trials. Analytical results (marked th) show a near-perfect match with the simulation results (marked sim).

Fig. 3 reports the results when the underlying networks have

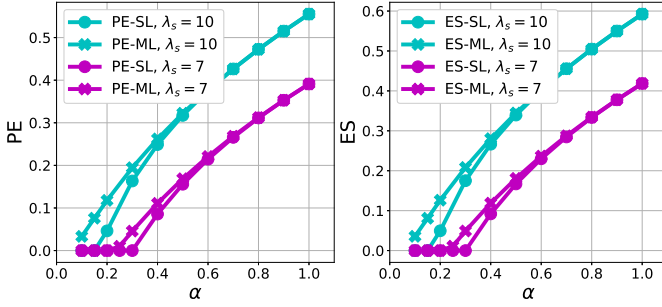


Fig. 4. Comparison of PE and ES for the multi-layer network model (abbrev. ML) and the single-layer projection (abbrev. SL) by degree projection. $\lambda_c = 7$, $T_c = 0.6$ and $T_s = 0.5$. Suppose there are only two types of masks with $\epsilon_{out} = [0.8, 0.5]$, $\epsilon_{in} = [0.7, 0.5]$. For the purpose of projection, we consider layer-independent population heterogeneity with mask type distribution $\mathbf{m}_{ML} = \mathbf{m}_{SL} = [0.4, 0.6]$.

their degree distribution following power law with exponential cutoff. There as well, we see a near-perfect match with a different type of degree distribution.

V. COMPARISON BETWEEN MULTI-LAYER AND SINGLE-LAYER NETWORKS

This section compares the dynamics of spreading processes over a single-layer network with that over a multi-layer network. In other words, we consider whether projecting a multi-layer network into a single-layer network leads to any significant differences in the dynamics that warrant a separate analysis of the multi-layer network structure. For simplicity, we assume the degree distribution of the contact network is Poisson.

As mentioned in Sec. II-A, we generate layer- \mathbb{S} and layer- \mathbb{C} separately based on the configuration model, with respective degree distributions $\{p_k^s\}$ and $\{p_k^c\}$. This results in the *colored* degree distribution as shown in (2). One approach to project the multi-layer network degree distribution to a single-layer network degree distribution is to *ignore* the color (i.e., edge type) of the edges and match all stubs randomly with each other. For example, if layer- \mathbb{C} has degree distribution $\text{Poisson}(\lambda_c)$ and baseline transmissibility T_c , and layer- \mathbb{S} has degree distribution $\text{Poisson}(\lambda_s)$ and baseline transmissibility T_s , the corresponding single-layer projection will have a degree distribution given by

$$p_{d_{SL}} = \begin{cases} \text{Poisson}(\lambda_c T_c) + \text{Poisson}(\lambda_s T_s) & \text{w.p. } \alpha \\ \text{Poisson}(\lambda_c T_c) & \text{w.p. } 1 - \alpha. \end{cases}$$

Here, w.p. is short for with probability and α denotes the probability that a node belongs to both layers.¹

Assuming there are two types of masks in the population for convenience, we consider layer-independent population heterogeneity for the multi-layer network model for the single-layer projection. Given the same mask efficiencies and distribution, we compare PE and ES for multi-layer (abbrev. ML)

¹Here, we use $\text{Poisson}(\lambda_c T_c)$ to represent the degree distribution of layer- \mathbb{C} after bond percolation with occupation probability T_c since $\text{Binomial}(n; p)$ with $np = \lambda$ converges in distribution to $\text{Poisson}(\lambda)$ as $n \rightarrow \infty$; and, if the original degree distribution is $\text{Binomial}(n; p)$, after bond percolation with occupation probability T_c , it becomes $\text{Binomial}(n; pT)$.

and projected single-layer (abbrev. SL) models. Fig. 4 shows the results when $\lambda_s = 7$ and 10 with fixed $\lambda_c = 7$ while varying α . We see that PE-SL and ES-SL do not match the corresponding ML results. First, the SL results are not able to accurately predict the epidemic threshold. Second, there is a discrepancy between ML and SL results. It is observed that when both PE-ML and PE-SL (ES-ML and ES-SL follow the same trend) are non-zero, increasing α decreases this discrepancy.

We now explain why there exists a discrepancy between ML and SL. The key difference between the ML and SL network models is the correlation between the degrees of the neighboring nodes. When α is small, for example, $\alpha = 0.1$, only 10% of the nodes have type- c edges, and they can only be randomly matched with other type- c edges in the ML case. In this case, a small fraction of the population will have statistically *higher* degrees than the rest, and the additional links they have only connect nodes with high degrees together. This results in a positive correlation, i.e., assortativity, between the degrees of pairs of connected nodes. High-degree nodes provide a higher probability of transmitting the spreading item to the rest compared to the low-degree nodes, and higher assortativity will amplify such an effect. This is also the reason that transition points of SL come later than ML as α increases, and the ML predictions for PE and ES are above the SL ones.

We further consider the case where the single-layer and multi-layer models match the spectral radius values $\rho(\mathbf{J})^2$ given by (13) and (14), because the degree projection method above does not match the transition points between SL and ML. Both (13) and (14) disentangle three impact factors on the critical transition behavior of a spreading process: a term that attributes the network structure, a term incorporating baseline transmissibilities, and a population heterogeneity term. This provides a direct method of projection that keeps the same spectral radius for ML and SL: given the same the population heterogeneity term, and letting

$$\frac{\langle k^2 \rangle - \langle k \rangle}{\langle k \rangle} \cdot T = \rho \left(\begin{bmatrix} T_c & \\ & T_s \end{bmatrix} \cdot \begin{bmatrix} \lambda_{cc} & \lambda_{cs} \\ \lambda_{sc} & \lambda_{ss} \end{bmatrix} \right).$$

Fig. 5 shows the results of the second projection method by matching spectral radius with varying α . We can see that even after matching spectral radius, SL can not accurately predict PE and ES. Similar to Fig. 4, when α increases, the difference between the predictions of SL and ML decreases in most cases.

In summary, we find that the projected single-layer network cannot accurately predict PE and ES for the corresponding multi-layer network when ignoring the edge type and aggregating the layers, as well as matching spectral radius. Thus the single-layer projection of a multi-layer network can not capture the essential properties (e.g., PE and ES) of a spreading process.

²In the special case where $M = 1$, it is also known as the *basic reproduction number*, R_0 , defined as the *secondary* infections in a *naive* population. It is known that if R_0 is greater than one then the PE is positive, i.e., epidemics can take place. When $R_0 \leq 1$, however, the PE is zero [9]. In fact authors of [16] defined and calculated R_0 for their heterogenous bond percolation model as a natural extension of the $M = 1$ case, yielding the same result shown in (14). In this paper, $\rho(\mathbf{J})$ is not exactly the basic reproduction number based on the definition, but it shares the same transition behavior at $\rho(\mathbf{J}) = 1$, and is able to obtain (14).

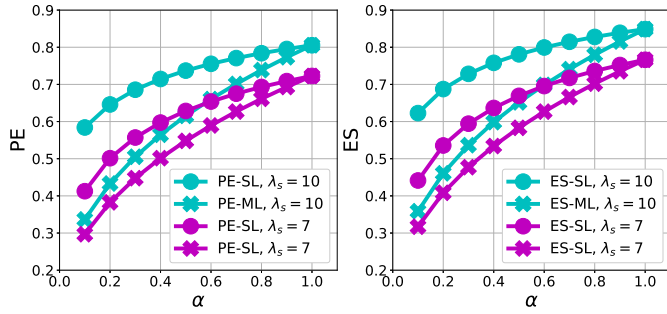


Fig. 5. Comparison of PE and ES for the multi-layer network model (abbrev. ML) and the single-layer projection (abbrev. SL) by matching spectral radius given by (13) and (14).

VI. LAYER-ORIENTED SPREADING CONTROL WITH LIMITED COST

Utilizing the layer-dependent population heterogeneity model, we develop and discuss three layer-oriented mask allocation strategies given certain constraints on the total *cost* of masks. We name the three strategies Policy 1, Policy 2, and Policy 3, respectively. As mentioned, the multi-layer contact network $\mathbb{H} = \mathbb{C} \parallel \mathbb{S}$ is composed of layer \mathbb{C} and layer \mathbb{S} , where nodes in the layer- \mathbb{C} participate in layer- \mathbb{S} with probability α . In this section, we assume there are two types of masks: mask and no-mask, labeled as mask type-1 and mask type-2. The outward and inward efficiencies are denoted by $\epsilon_{\text{out}} = [\epsilon_{\text{out},1}, \epsilon_{\text{out},2}]$, and $\epsilon_{\text{in}} = [\epsilon_{\text{in},1}, \epsilon_{\text{in},2}]$, where $0 < \epsilon_{\text{out},1}, \epsilon_{\text{in},1} \leq 1$ and $\epsilon_{\text{out},2} = \epsilon_{\text{in},2} = 0$. Similar to Sec. IV, the entire population is split into four non-overlapping categories. Policy 1 provides a baseline where each node in \mathcal{N} has consistent mask-wearing behavior across the two layers of the contact network. Policy 2 explores a case where nodes do not wear masks over layer- \mathbb{S} . In contrast, Policy 3 requires masks to be mandated over layer- \mathbb{S} . More specifically, let $\mathbf{m}^\pi = [m_{11}^\pi, m_{21}^\pi, m_{12}^\pi, m_{22}^\pi]$ denote the proportion of the above 4 categories for Policy π , where $\pi = 1, 2, 3$. Policy 1 has $\mathbf{m}^1 = [m_{11}^1, 0, 0, m_{22}^1]$ where $m_{11}^1 + m_{22}^1 = 1$; Policy 2 has $\mathbf{m}^2 = [0, m_{12}^2, 0, m_{22}^2]$, $m_{12}^2 + m_{22}^2 = 1$; Policy 3 has $\mathbf{m}^3 = [m_{11}^3, 0, m_{21}^3, 0]$ and $m_{11}^3 + m_{21}^3 = 1$.

To quantify the expected total cost of policy π spending on masks for a fair comparison among the three policies, we propose the below formula:

$$\mathbb{E}[\text{cost}^\pi] = \sum_{i,j=1}^M \mathbb{E}[\text{cost}_{ij}^\pi] \cdot m_{ij}^\pi \quad (19)$$

where $i, j = 1, \dots, M$ and $\pi = 1, 2, 3$. $\mathbb{E}[\text{cost}_{ij}^\pi]$ denotes the expected cost for a type- ij individual, which is independent of the spreading process and the policies. In the considered case where $M = 2$, we have $\mathbb{E}[\text{cost}_{11}^\pi] = 1 + \alpha$, $\mathbb{E}[\text{cost}_{12}^\pi] = 1$, $\mathbb{E}[\text{cost}_{21}^\pi] = \alpha$, and $\mathbb{E}[\text{cost}_{22}^\pi] = 0$.

With these in hand, we investigate two problems in turn: (i) Given a budget of C for the cost of masks, i.e., let $\mathbb{E}[\text{cost}^1] = \mathbb{E}[\text{cost}^2] = \mathbb{E}[\text{cost}^3] = C$, which policy yields the *best* mitigation effect (i.e., the lowest PE of an epidemic)? (ii) To prevent the epidemic from happening, which policy yields the *lowest* expected cost?

A. PE with the same expected cost

Next, we compare the effectiveness of different policies for mitigating the spreading which is measured by reduction in PE. In what follows, for simplicity, we generate the networks using Poisson degree distributions. Fig. 6 shows the results for Policy 1, 2 and 3 when their expected costs are the same, as we increase m_{11}^1 from 0.1 to 0.9 when $\alpha = 0.1$ and $\alpha = 0.9$. Given m_{11}^1 (x-axis), we have $\mathbf{m}^1 = [m_{11}^1, 1 - m_{11}^1, 0, 0]$. $C = \mathbb{E}[\text{cost}^1]$ can be obtained via (19). With $\mathbb{E}[\text{cost}^2] = \mathbb{E}[\text{cost}^3] = C$, we can solve for m_{12}^2 and m_{21}^3 . We note that it is not guaranteed to have valid solutions (i.e., in the range $[0, 1]$) for m_{12}^2 and m_{21}^3 . If the solutions have negative values, we replace them with 0s, and similarly, if they are larger than 1, we replace them with 1s. As shown in Fig. 6(a), when $\alpha = 0.1$, given m_{11}^1 and thus C , we can match $\mathbb{E}[\text{cost}^2] = \mathbb{E}[\text{cost}^3] = C$ by varying m_{11}^1 . However, in Fig. 6(b), when $\alpha = 0.9$, $\mathbb{E}[\text{cost}^3]$ can not always be made exactly C , e.g., if $m_{11}^1 < 0.5$ because it is lower-bounded by α . Similarly, when $m_{11}^1 > 0.5$, $\mathbb{E}[\text{cost}^2]$ reaches the upper bound 1 and can not be made exactly C .

Now we compare PE^1 , PE^2 , and PE^3 considering the different matching conditions for the expected costs as shown in Fig. 6(a) and 6(b). To explore the effectiveness of layer-dependent mask assignment policies, we further take into account the *transmission power* of each layer. Inspired by (14), we roughly estimate the *transmission power* of each layer by the product of the first moment of the degree distribution that generates the contact network layer and the baseline transmissibility of that layer, With $\text{Poisson}(\lambda_c)$ generating layer- \mathbb{C} and $\text{Poisson}(\lambda_s)$ generating layer- \mathbb{S} in this analysis, we consider three cases: (i) $T_c \lambda_c = T_s \lambda_s$; (ii) $T_c \lambda_c = 10 T_s \lambda_s$; (iii) $10 T_c \lambda_c = T_s \lambda_s$. The results are shown in Fig. 7.

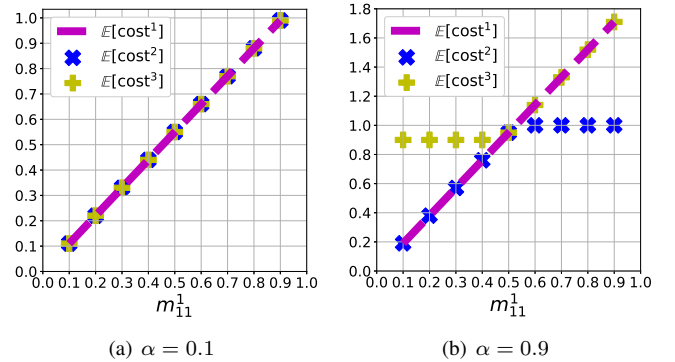


Fig. 6. $\mathbb{E}[\text{cost}^1]$ (dashed line), $\mathbb{E}[\text{cost}^2]$ (cross) and $\mathbb{E}[\text{cost}^3]$ (plus) with varying m_{11}^1 when $\alpha = 0.1$ (a), and $\alpha = 0.9$ (b).

In Fig. 7, we can see that the transmission power is a significant factor in determining the best control policy. It is more effective for a layer-oriented policy to direct more masks to the layer that has higher transmission power. When the transmission power of layer- \mathbb{C} is larger than layer- \mathbb{S} , as shown in Fig. 7(c) and 7(d), Policy 2 that directs as many masks as possible has the lowest PE for most cases. Only at $m_{11}^1 = 0.9$ when $\alpha = 0.9$, $\text{PE}^1 < \text{PE}^2$ due to $\mathbb{E}[\text{cost}^2]$ reaching the upper bound of 1. When $0.5 < m_{11}^1 < 0.9$ in Fig. 7(d), even with a lower expected cost than Policy 1 and 3, Policy 2 yields the lowest PE among all. Similarly, in Fig.

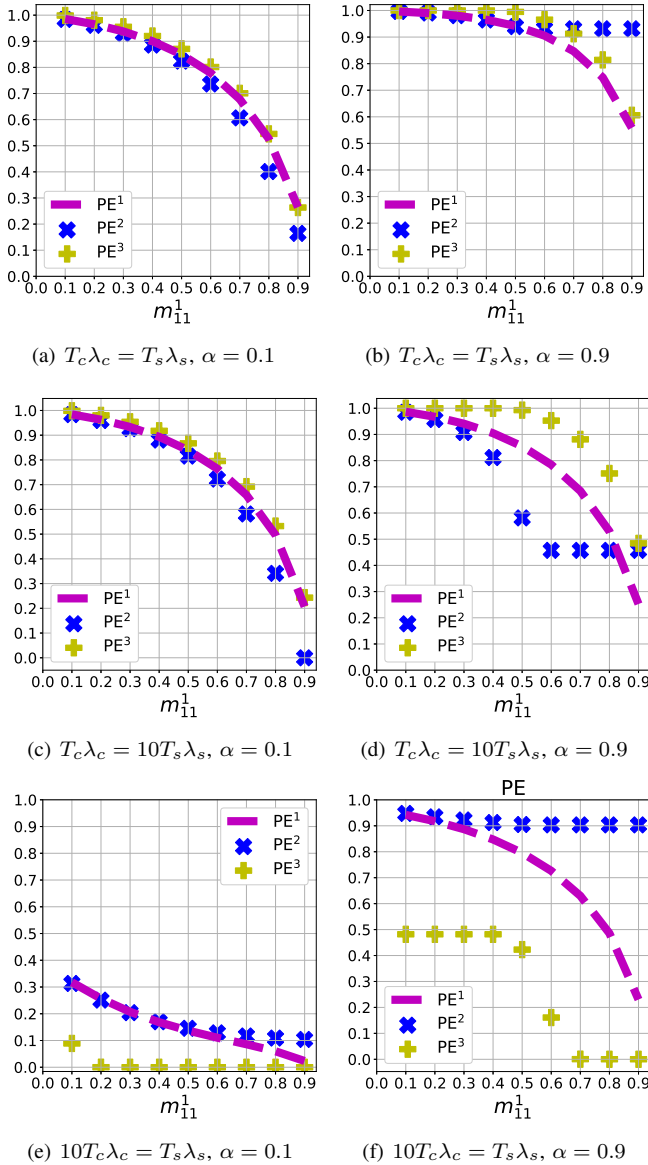


Fig. 7. PE^1 (dashed line), PE^2 (cross) and PE^3 (plus) with varying m_{11}^1 . Throughput $T_c = T_s = 0.5$, and $\epsilon_{out} = \epsilon_{in} = [0.8, 0]$. For (a) and (b), $\lambda_c = \lambda_s = 20$. For (c) and (d), $\lambda_c = 20, \lambda_s = 2$. For (e) and (f), $\lambda_c = 2, \lambda_s = 20$.

7(e) and 7(f), when layer-S has a higher transmission power, Policy 3 that mandates masks on layer-S is the best mitigation policy. When layer-C and layer-S share the same transmission power, as shown in Fig.7(a) and Fig.7(b), there is no single policy that outperforms others as α increases. In the specific case of Fig. 7(a), Policy 2 shows slightly lower PE than the other two policies, potentially due to the small participation rate of layer-S and equal transmission power of the two layers. Therefore the contribution to the spreading process of layer-S is not as significant as layer-C, which can also be seen from the comparison with Fig. 7(e). However, in Fig. 7(b) where $\alpha = 0.9$, when the two layers are more coupled, due to the same transmission power of the two layers, the baseline Policy 1, which favors neither layer, yields the lowest PE. Moreover, Fig. 7 shows that, when the transmission power of layers are different, increasing α increases the discrepancy of PE between the best policy and others. This indicates that

with a cost, when layer-S has a higher participation rate, it is particularly important to consider layer-oriented spreading control policies based on the transmission power of different layers.

B. The impact of expected cost on epidemic boundaries

Next, we discuss a different problem from that in Sec. VI-A, where we aim to find the optimal resource allocation strategy with a given budget. Here, our primary goal is to find a policy that prevents the epidemic from happening at the lowest cost. In particular, we need to find the expected costs for each policy at the corresponding *epidemic boundary*, i.e., the region in the parameter space identified by the epidemic threshold $\rho(\mathbf{J}) = 1$. Fig. 8 shows the boundary of $m - \alpha$ plane for Policy 1, 2 and 3 when the transmission power of layer-C is equal to, greater than, and less than that of layer-S.

On the LHS of each panel in Fig. 8, for each policy $\pi, \pi = 1, 2, 3$, the curves separate the areas where epidemics can take place (north-east of the curves) from the areas where they can not (south-west of the curves). Here we explore the trade-off between α and m_{ij}^π on the epidemic boundary where $\rho(\mathbf{J}) = 1$ while fixing other parameters. For clarity, we are only showing $\alpha - m_{22}^1$ plane for Policy 1, $\alpha - m_{22}^2$ plane for Policy 2, and $\alpha - m_{21}^3$ plane for Policy 3. For example, in the $\alpha - m_{22}^1$ plane in Fig. 8(a), for Policy 1, consider two types of nodes type-11 and type-22 where $m_{11}^1 + m_{22}^1 = 1$, and $\mathbb{E}[\text{cost}_{11}] = 0, \mathbb{E}[\text{cost}_{22}] = 1 + \alpha$. As α increases, the maximum fraction of nodes that can wear no mask on both layers such that epidemics are not possible decreases. In fact, in all $\alpha - m_{ij}^\pi$ planes in Fig. 8, regardless of the transmission power of the layers, increasing α decreases the maximum fraction of less-cost node types for a policy that is needed for epidemics to not happen.

In Fig. 8(c), when the transmission power of the secondary layer S is higher, it is also more *economical* (i.e., lower expected cost) to control layer-S. However, in Fig. 8(b), when the transmission power of layer-C is higher, controlling layer-S takes the least cost. These two trends echo our conclusions in Sec. VI-A that given a total cost, it is more effective to assign more masks to the layer that has higher transmission power. Most interestingly, in Fig. 8(a), when the transmission power of the two layers is the same, it is most economical to prioritize controlling the spreading on the layer-S to prevent the epidemic, as shown by results of Policy 3. First, on the LHS, Policy 3 allows more fractions of less-cost node types in the population. Meanwhile, on the RHS, Policy 3 also spends the least expected costs compared to other policies. This is likely due to the fact that the second layer provides extra transmission pathways and thus increases the connectivity of the contact network, which makes it critical to block the transmission over the second layer to prevent the epidemic from happening.

VII. CONCLUSIONS

In this work, we provide a comprehensive analysis of the spreading process in multi-layer networks with layer-dependent population heterogeneity. We present analytical

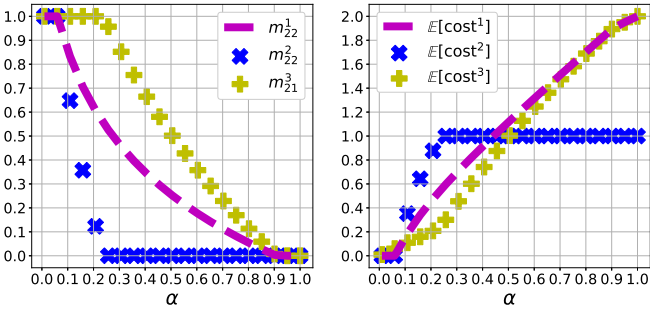
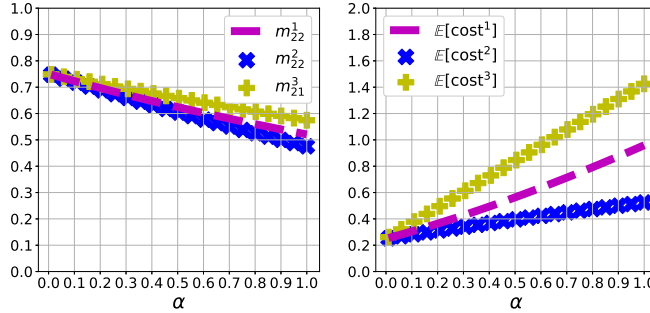
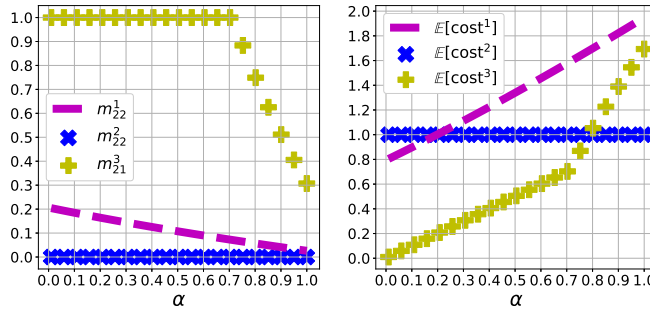

 (a) $T_c \lambda_c = T_s \lambda_s$

 (b) $T_c \lambda_c = 10 T_s \lambda_s$

 (c) $10 T_c \lambda_c = T_s \lambda_s$

Fig. 8. Epidemic boundaries of $\alpha - m_{ij}^p$ planes (LHS) and the corresponding $\mathbb{E}[\text{cost}^p]$ (RHS) on the epidemic boundaries. Policy 1, 2 and 3 correspond to dashed lines, cross and plus, respectively. Each curve in $\alpha - m_{ij}^p$ planes is the epidemic boundary identified by $\rho(\mathcal{J}) = 1$ for a policy when considering the trade-off between α and the fraction of the nodes whose node types have less cost for that policy. The north and east of each curve in $\alpha - m_{ij}^p$ planes specify the region for which epidemics are possible, while the south and west parts of each curve stand for the region where epidemics can not occur. Each policy's corresponding expected costs on the epidemic boundary are provided on its RHS. Throughout $\epsilon_{out} = \epsilon_{in} = [0.8, 0]$. For (a), $T_c = 0.2, T_s = 1, \lambda_c = 4, \lambda_s = 0.8$. For (b), $T_c = 0.05, T_s = 0.5, \lambda_c = 22, \lambda_s = 0.22$. For (c), $T_c = 0.2, T_s = 1, \lambda_c = 0.7, \lambda_s = 1.4$.

solutions for three key epidemiological measures: probability of emergence (PE), epidemic threshold, and expected epidemic size (ES). Our solutions disentangle the impact of multi-layer network structure, transmission dynamics, and population heterogeneity distribution on the final state of the spreading process. We validate our analytical results with extensive simulations. Comparing multi-layer networks to their single-layer projections, we find significant differences in the dynamics, emphasizing the need for separate analysis of multi-layer structures. We also explore the impact of layer-dependent population heterogeneity by studying three layer-oriented mitigation control policies. We propose a metric to

quantify the expected cost of mask allocation, which helps characterize different policies. We identify the transmission power of each layer and the participation rate of nodes in the secondary layer as crucial factors for developing effective and economical mitigation strategies. Our findings provide insights into the spreading process in multi-layer complex networks with population heterogeneity and can help develop mitigation and control strategies for disease spread and information diffusion.

REFERENCES

- [1] Y. Tian and O. Yağan, “Spreading processes with population heterogeneity over multi-layer networks,” Nov. 2022. Available at <http://arxiv.org/abs/2211.07479>.
- [2] M. Tambuscio, G. Ruffo, A. Flammini, and F. Menczer, “Fact-checking Effect on Viral Hoaxes: A Model of Misinformation Spread in Social Networks,” in *Proceedings of the 24th International Conference on World Wide Web, WWW '15 Companion*, 2015.
- [3] H. W. Hethcote, “The Mathematics of Infectious Diseases,” *SIAM Review*, vol. 42, no. 4, 2000. Publisher: Society for Industrial and Applied Mathematics.
- [4] J. P. Gleeson and D. J. Cahalane, “Seed size strongly affects cascades on random networks,” *Physical Review E*, vol. 75, no. 5, 2007.
- [5] M. Newman, “Epidemics on networks,” in *Networks* (M. Newman, ed.), 2018.
- [6] M. Li, X. Wang, K. Gao, and S. Zhang, “A Survey on Information Diffusion in Online Social Networks: Models and Methods,” *Information*, vol. 8, no. 4, 2017.
- [7] A. Allard, P.-A. Noël, L. Dubé, and B. Pourbohloul, “Heterogeneous Bond Percolation on Multitype Networks with an Application to Epidemic Dynamics,” *Physical review E, Statistical, nonlinear, and soft matter physics*, vol. 79, 2009.
- [8] O. Yağan, D. Qian, J. Zhang, and D. Cochran, “Conjoining Speeds up Information Diffusion in Overlaying Social-Physical Networks,” *IEEE Journal on Selected Areas in Communications*, vol. 31, no. 6, 2013.
- [9] M. E. J. Newman, “Spread of epidemic disease on networks,” *Physical Review E*, vol. 66, no. 1, 2002.
- [10] P. Grassberger, “On the critical behavior of the general epidemic process and dynamical percolation,” *Mathematical Biosciences*, vol. 63, no. 2, 1983.
- [11] Y. Zhuang and O. Yağan, “Information propagation in clustered multi-layer networks,” *IEEE Transactions on Network Science and Engineering*, vol. 3, no. 4, pp. 211–224, 2016.
- [12] M. E. Newman, “Random graphs with clustering,” *Physical review letters*, vol. 103, no. 5, p. 058701, 2009.
- [13] J. C. Miller, “Percolation and epidemics in random clustered networks,” *Physical Review E*, vol. 80, no. 2, p. 020901, 2009.
- [14] C. Buono, L. G. Alvarez-Zuzek, P. A. Macri, and L. A. Braunstein, “Epidemics in Partially Overlapped Multiplex Networks,” *PLOS ONE*, vol. 9, no. 3, 2014.
- [15] A. Hackett, D. Cellai, S. Gómez, A. Arenas, and J. Gleeson, “Bond Percolation on Multiplex Networks,” *Physical Review X*, vol. 6, p. 021002, Apr. 2016.
- [16] Y. Tian, A. Sridhar, C. W. Wu, S. A. Levin, K. M. Carley, H. V. Poor, and O. Yağan, “Role of masks in mitigating viral spread on networks,” *Phys. Rev. E*, vol. 108, p. 014306, Jul 2023.
- [17] X. Chen, G. Zhu, L. Zhang, Y. Fang, L. Guo, and X. Chen, “Age-Stratified COVID-19 Spread Analysis and Vaccination: A Multitype Random Network Approach,” *IEEE transactions on network science and engineering*, vol. 8, no. 2, 2021.
- [18] Y. Tian, A. Sridhar, O. Yağan, and H. V. Poor, “Analysis of the Impact of Mask-wearing in Viral Spread: Implications for COVID-19,” in *2021 American Control Conference (ACC)*, pp. 3132–3137, May 2021. ISSN: 2378-5861.
- [19] D.-S. Lee and M. Zhu, “Epidemic Spreading in a Social Network with Facial Masks wearing Individuals,” *IEEE Transactions on Computational Social Systems*, vol. 8, no. 6, 2021.
- [20] G. Bonifazi, B. Breve, S. Cirillo, E. Corradini, and L. Virgili, “Investigating the COVID-19 vaccine discussions on Twitter through a multi-layer network-based approach,” *Information Processing & Management*, vol. 59, no. 6, 2022.

- [21] G. J. Milne, J. K. Kelso, H. A. Kelly, S. T. Huband, and J. McVernon, "A Small Community Model for the Transmission of Infectious Diseases," *Plos One*, vol. 3, no. 12, 2008.
- [22] C. Bongiorno and L. Zino, "A multi-layer network model to assess school opening policies during a vaccination campaign," *Applied Network Science*, vol. 7, no. 1, 2022.
- [23] "2022 school mask guide," 2022. <https://www.cbsnews.com/pittsburgh/news/2022-school-mask-guide/>.
- [24] M. Molloy, "A Critical Point For Random Graphs With A Given Degree Sequence,"
- [25] M. E. J. Newman, S. H. Strogatz, and D. J. Watts, "Random graphs with arbitrary degree distributions and their applications," *Physical Review E*, vol. 64, no. 2, 2001.
- [26] J. W. Chun and M. J. Lee, "When does individuals' willingness to speak out increase on social media? Perceived social support and perceived power/control," *Computers in Human Behavior*, vol. 74, pp. 120–129, Sept. 2017.
- [27] J. R. Silvester, "Determinants of block matrices," *The Mathematical Gazette*, vol. 84, no. 501, p. 460–467, 2000.
- [28] R. Eletreby, Y. Zhuang, K. M. Carley, O. Yağan, and H. V. Poor, "The effects of evolutionary adaptations on spreading processes in complex networks," *Proceedings of the National Academy of Sciences*, vol. 117, no. 11, 2020.
- [29] B. Söderberg, "Properties of random graphs with hidden color," *Physical Review E, Statistical, Nonlinear, and Soft Matter Physics*, vol. 68, no. 2 Pt 2, 2003.
- [30] E. A. Leicht and R. M. D'Souza, "Percolation on interacting networks," July 2009. arXiv:0907.0894 [cond-mat].
- [31] P. Yang *et al.*, "Mask-wearing and respiratory infection in healthcare workers in beijing, china," *The Brazilian Journal of Infectious Diseases*, vol. 15, no. 2, pp. 102–108, 2011.
- [32] M. v. d. Sande, P. Teunis, and R. Sabel, "Professional and home-made face masks reduce exposure to respiratory infections among the general population," *PLOS ONE*, vol. 3, no. 7, p. e2618, 2008.
- [33] K. Athreya and P. Ney, *Branching Processes*, vol. 196. 1972.

AUTHOR BIOGRAPHIES



Yurun Tian received the M.S. in Electrical and Computer Engineering (ECE) from Carnegie Mellon University (CMU) in 2021. She is currently working towards the Ph.D. degree in ECE, CMU, Pittsburgh, PA, USA.



Osman Yağan is a Research Professor of ECE at CMU. Dr. Yağan received his Ph.D. degree in ECE from the University of Maryland at College Park, MD in 2011. Dr. Yağan is a recipient of a CIT Dean's Early Career Fellowship, an IBM Academic Award, and best paper award in ICC 2021 and IPSN 2022.

APPENDIX A

CONVERGENCE AND PHASE TRANSITION OF ES

We remark that the convergence to the fixed point $\mathbf{q}_{c,\infty}$ and $\mathbf{q}_{s,\infty}$ is guaranteed. Namely, taking the limit $\ell \rightarrow \infty$ in (15) - (18) is a well-defined operation since the multi-type branching process corresponding to (15) and (16) is positive regular and non-singular under the assumption that $m_{ij} > 0$, $\mathbf{T}_c[i, j] > 0$, $\mathbf{T}_s[i, j] > 0$ for all integers $1 \leq i, j \leq M$. Then the convergence to the fixed point $\mathbf{q}_{c,\infty}$ and $\mathbf{q}_{s,\infty}$ is guaranteed as long as the initial condition $\mathbf{q}_{c,0}$ and $\mathbf{q}_{s,0}$ have positive entries [33, Theorem V.3.2], which hold under the condition the epidemic emerges.

Just as in the PE, there is a phase transition between ES being zero ($\mathbf{q}_{c,\infty} = \mathbf{1}$, $\mathbf{q}_{s,\infty} = \mathbf{1}$) and ES being positive ($\mathbf{q}_{c,\infty} < \mathbf{1}$, $\mathbf{q}_{s,\infty} < \mathbf{1}$). Similar to (8) and (16). Let \mathbf{J}' denote the Jacobian matrix of relations (15) and (16), we show the threshold for the ES is given by $\rho(\mathbf{J}') = 1$ where

$$\mathbf{J}' = \begin{bmatrix} \mathbf{J}'_{cc} & \mathbf{J}'_{cs} \\ \mathbf{J}'_{sc} & \mathbf{J}'_{ss} \end{bmatrix}_{2M^2 \times 2M^2} \quad \text{with}$$

$$\begin{aligned} \mathbf{J}'_{cc}(a, b) &= \frac{\partial q_{c,\infty}^{ij}(1)}{\partial q_{c,\infty}^{rt}(1)}; & \mathbf{J}'_{cs}(a, b) &= \frac{\partial q_{c,\infty}^{ij}(1)}{\partial q_{s,\infty}^{rt}(1)} \\ \mathbf{J}'_{ss}(a, b) &= \frac{\partial q_{s,\infty}^{ij}(1)}{\partial q_{s,\infty}^{rt}(1)}; & \mathbf{J}'_{sc}(a, b) &= \frac{\partial q_{s,\infty}^{ij}(1)}{\partial q_{c,\infty}^{rt}(1)} \end{aligned} \quad (20)$$

where $a = \text{M2D}(i, j), b = \text{M2D}(r, t); 1 \leq i, j, r, t \leq M$. More specifically,

$$\begin{aligned} \mathbf{J}'_{cc} &= [\lambda_{cc} \cdot \mathbf{T}'_c{}^\top \cdot \mathbf{m}]; & \mathbf{J}'_{cs} &= [\lambda_{cs} \cdot \mathbf{T}'_c{}^\top \cdot \mathbf{m}] \\ \mathbf{J}'_{sc} &= [\lambda_{sc} \cdot \mathbf{T}'_s{}^\top \cdot \mathbf{m}]; & \mathbf{J}'_{ss} &= [\lambda_{ss} \cdot \mathbf{T}'_s{}^\top \cdot \mathbf{m}] \end{aligned} \quad (21)$$

When $\rho(\mathbf{J}')$ is less than or equal to 1, $\mathbf{q}_{c,\infty} = \mathbf{1}$, $\mathbf{q}_{s,\infty} = \mathbf{1}$. When $\rho(\mathbf{J}')$ is greater than 1, $q_{c,\infty}^{ij}, q_{s,\infty}^{ij} < 1$ for all $1 \leq i, j \leq M$. It can be seen that \mathbf{J}' shares the exactly same transition points defined by $\rho(\mathbf{J}) = 1$.

We show this by proving \mathbf{J}^\top and \mathbf{J}' have the same spectrum, which in turn implies that $\rho(\mathbf{J}) = \rho(\mathbf{J}')$ because $\rho(\mathbf{J}) = \rho(\mathbf{J}^\top)$. Note that \mathbf{J}^\top has the following form: $\mathbf{J}^\top = \begin{bmatrix} \mathbf{J}^{\top}_{cc} & \mathbf{J}^{\top}_{sc} \\ \mathbf{J}^{\top}_{cs} & \mathbf{J}^{\top}_{ss} \end{bmatrix}$ where

$$\begin{aligned} \mathbf{J}^{\top}_{cc} &= [\lambda_{cc} \cdot \mathbf{T}'_c{}^\top \cdot \mathbf{m}]; & \mathbf{J}^{\top}_{cs} &= [\lambda_{cs} \cdot \mathbf{T}'_c{}^\top \cdot \mathbf{m}] \\ \mathbf{J}^{\top}_{sc} &= [\lambda_{sc} \cdot \mathbf{T}'_s{}^\top \cdot \mathbf{m}]; & \mathbf{J}^{\top}_{ss} &= [\lambda_{ss} \cdot \mathbf{T}'_s{}^\top \cdot \mathbf{m}] \end{aligned} \quad (22)$$

The only difference between (22) and (21) is the anti-diagonal blocks (left-bottom to upper-right) swapping the positions. This can be seen through the stronger property that the characteristic polynomials of the two matrices are identical. Specifically, based on Theorem 3 of the determinant of block matrix in Ref. [27], for block matrix (11), where $\mathbf{J}_{sc}\mathbf{J}_{ss} = \mathbf{J}_{ss}\mathbf{J}_{sc}$, we have $\det(\mathbf{J}) = \det(\mathbf{J}_{cc}\mathbf{J}_{ss} - \mathbf{J}_{cs}\mathbf{J}_{sc}) = \det(\mathbf{J}^{\top}_{ss}\mathbf{J}^{\top}_{cc} - \mathbf{J}^{\top}_{sc}\mathbf{J}^{\top}_{cs})$. Similarly, due to $\mathbf{J}'_{cc}\mathbf{J}'_{cs} = \mathbf{J}'_{cs}\mathbf{J}'_{cc}$, $\det(\mathbf{J}') = \det(\mathbf{J}^{\top}_{ss}\mathbf{J}^{\top}_{cc} - \mathbf{J}^{\top}_{sc}\mathbf{J}^{\top}_{cs})$. Putting together the results of this section and Section III-A, we have shown that when $\rho(\mathbf{J}) \leq 1$, the epidemic dies out in finite time, whereas when $\rho(\mathbf{J}) > 1$, the epidemic eventually infects a positive fraction of the population.